Noname manuscript No.
(will be inserted by the editor)

High-Velocity Operation of Piezoelectric Inertia Motors – Experimental Validation

Matthias Hunstig · Tobias Hemsel · Walter Sextro

Author's accepted manuscript – The final publication is available at Springer via http://dx.doi.org/10.1007/s00419-014-0940-0.

Abstract Piezoelectric inertia motors use the inertia of a body to drive it by means of a friction contact in a series of small steps. It has been shown previously in theoretical investigations that higher velocities and smoother movements can be obtained if these steps do not contain phases of stiction ("stick-slip" operation), but use sliding friction only ("slip-slip" operation). One very promising driving option for such motors is the superposition of multiple sinusoidal signals or harmonics. In this contribution, the theoretical results are validated experimentally. In this context, a quick and reliable identification process for parameters describing the friction contact is proposed. Additionally, the force generation potential of inertia motors is investigated theoretically and experimentally. The experimental results confirm the theoretical result that for a given maximum frequency, a signal with a high fundamental frequency and consisting of two superposed sine waves leads to the highest velocity and the smoothest motion while the maximum motor force is obtained with signals containing more harmonics. These results are of fundamental importance for the further development of high-velocity piezoelectric inertia motors.

Keywords inertia motor · high velocity · stick-slip motor · slip-slip operation · friction parameter identification

1 Introduction

Piezoelectric inertia motors have originally been developed in the mid-1980s for fine positioning in microscopy applications [1, 10, 24]. Facilitated by the fact that they have a simple construction and are controlled by a single signal, which allows for low production costs and simplifies miniaturization, inertia motors have been applied in several

M. Hunstig, T. Hemsel, W. Sextro
Mechatronics and Dynamics, University of Paderborn, Pohlweg 47–49, 33098 Paderborn, Germany
Tel.: +49-5251-601805
Fax: +49-5251-601803
E-mail: tobias.hemsel@upb.de

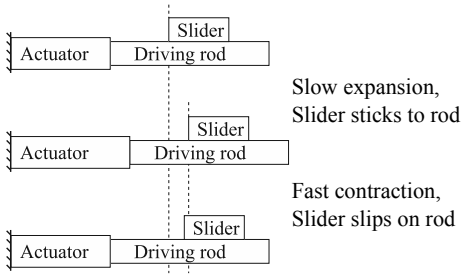

Fig. 1 Classic inertia motor operation cycle

other fields in the last years, often in miniaturized consumer goods [9,16,17,22,28]. In such applications, criteria like the motor velocity or its power consumption and lifetime are much more important than in classic microscopy applications.

All these motors use the inertia of a body to drive it by means of a friction contact in a series of small steps. The steps are classically assumed to consist of alternating phases of stiction and sliding, which is why inertia motors are also known as "stick-slip-drives". Fig. 1 illustrates one movement cycle of an inertia motor with a fixed stator.

But inertia motors can also operate without phases of stiction. Different researchers have presented inertia motors using such a "slip-slip" mode of operation in the last years, e. g. in [16,18,19,20,21,27]. The principal advantages, disadvantages and limitations of these two modes of operation have been investigated recently using a theoretical model [14,15]. The following section gives a short summary of the theoretical findings. For their experimental validation, a test motor has been set up, which is described in section 3. Section 4 introduces the model used for its simulation. Because inertia motors operate through friction, an appropriate characterization of the friction contact is crucial for a valid motor model. Section 5 describes the experiments performed to characterize the friction contact. Section 6 explains the experimental setup for the operational experiments, during which different motor parameters have been measured. In section 7, experimental results are described and compared to simulation results. Section 8 closes this contribution with a short summary and conclusions for further developments of high-velocity inertia motors.

2 Drive signals for high-velocity inertia motors

Inertia motors can be driven with a large variety of drive signals. A theroetical investigation of the idealized operation of inertia motors [14] has shown that there are four principally different operation modes of inertia motors, differentiated by two criteria: Does the slider move in discrete steps or continuously and is the propulsion of the slider achieved using stiction or by sliding friction only? The motor velocity in stick-slip operation and/or with discrete steps is limited principally, only continuous slip-slip operation allows very high velocities. To achieve the highest possible velocity, the displacement profile x_R of the stator of an inertia motor would ideally be a "parabolic sawtooth" signal as shown in fig. 2, repeated at a high frequency and with a large stroke [14].

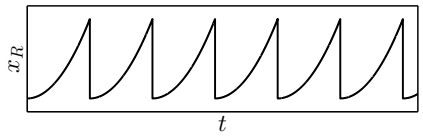

Fig. 2 Ideal stator movement pattern for high motor velocity

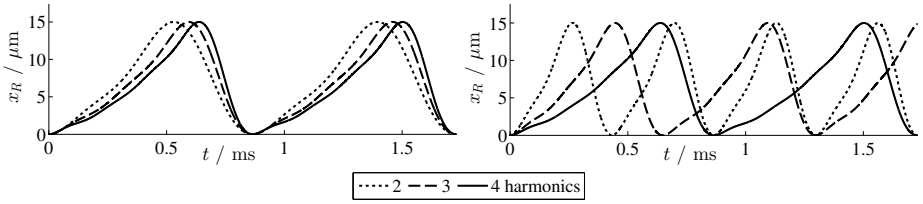

Fig. 3 Drive signals derived from the parabolic sawtooth signal in fig. 2, composed of n harmonics, with a) the same fundamental frequency $f_1 = 1156\,\mathrm{Hz}$, b) the same maximum frequency $f_n = n \cdot f_1 = 4625\,\mathrm{Hz}$

Such sawtooth signals with their – ideally infinitely – steep flanks are hard to obtain with a real actuator, especially at high fundamental frequencies. One very promising alternative drive signal for high-velocity inertia motors is the superposition of multiple sinusoidal signals, i. e. harmonics. Such signals contain only a few frequencies and thus do not require high-bandwidth actuators. They have been sucessfully used in inertia motors by different researchers. In appropriately designed motors, these drive signals can make use of resonant amplification to achieve large stator amplitudes and thus high velocities [2,20,18,19], even with electrical excitation amplitudes as low as 0.8 V [19].

In [15], frequency-limited signals composed of different numbers of harmonics were derived from the ideal signals shown in fig. 2 using Fourier series and Lanczos' σ factors [8, pp. 534–538] to reduce undesired vibrations. Fig. 3 shows examples of such signals with 2, 3, and 4 superposed harmonics.

With a transducer of limited bandwidth, a trade-off between a high fundamental drive frequency and a large number of harmonics has to be made. Simulations documented in [15] show that, with a given frequency f_n of the highest harmonic, the highest velocity and the smoothest motion are achieved when the motor is driven with a signal containing only two harmonics. With this signal, the motor also reaches the highest velocity per electrical input power. Recent investigations [11] show that the force generation potential of an inertia motor is largely independent of the drive frequency, but can be increased significantly by using a drive signal containing more than two harmonics.

3 Design of a test motor

In order to validate the above-mentioned theoretical results, a test motor has been built, which is capable of operating with the same stator amplitude at different frequencies and numbers of harmonics. Resonant inertia motors provide high velocities at low electric excitation amplitudes, but they are not suitable for the experiments

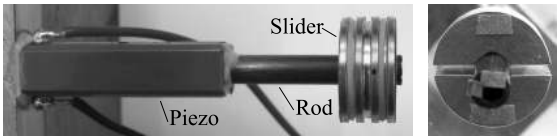

Fig. 4 Test motor – top view (left) and front view (right)

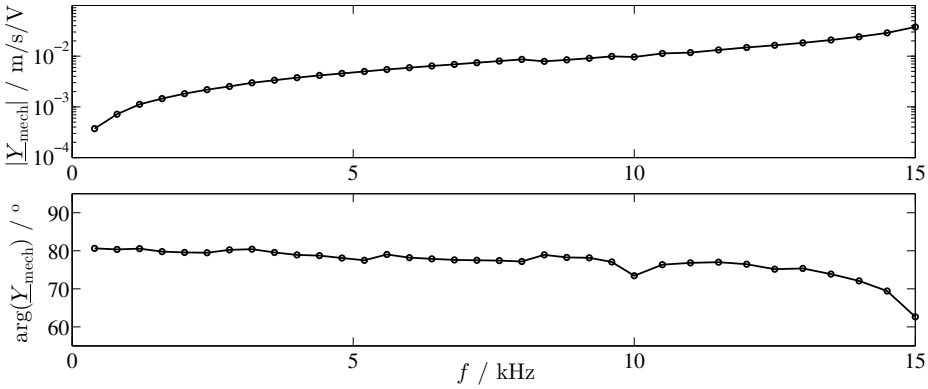

Fig. 5 Frequency sweep of amplitude and phase of the "mechanical admittance" $\underline{Y}_{\mathrm{mech}} = \dot{x}_R/u$ of the stator without slider

because they can operate properly only at one fixed fundamental frequency and with two harmonics. Instead, a motor has been constructed whose operation is unimpaired by any resonant effects at frequencies up to more than 10 kHz. Its stator consists of a piezoelectric multilayer actuator with a rod made of carbon fibre reinforced plastic glued to one of its ends. The other end of the piezoelectric actuator is glued to a massive steel block. A cylindrical brass slider moves along the rod. It is cut into two halves which are held together by rubber bands providing the normal force in the friction contact. Fig. 4 shows photographs of the motor. It has a total length of about 52 mm, the slider has a mass of 6.92 g.

Figure 5 shows a frequency sweep of the "mechanical admittance" $\underline{Y}_{\mathrm{mech}}$, i. e. the relation of the velocity of the rod tip $\dot{x}_R$ and the excitation voltage u. Measurements of the surface velocity along the rod have shown that it is approximately the same at each point. The rod can thus be regarded as a rigid body.

4 Motor model

The rigid body model shown in fig. 6 is used to simulate the motor operation: $x_R(t)$ and $x_S(t)$ are the displacements of rod and slider, respectively; m_S is the slider mass. The contact force $F_c(t)$ between rod and slider results from the gravitational force $F_g = m_S g$, where $g = 9.81\,\mathrm{m/s^2}$ is the gravitational constant, and an external force $F_z(t)$, both assumed to act on the center of gravity C of the slider. The friction force $F_f(t)$ acts between rod and slider. An additional force $F_x(t)$ acts on the slider in positive direction of x_S.

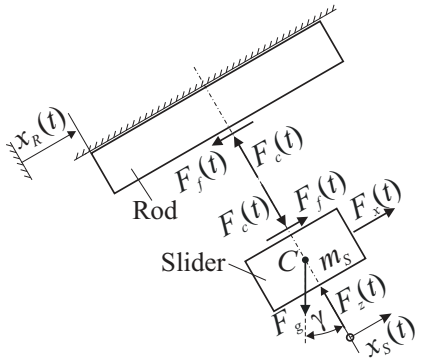

Fig. 6 Rigid body model of the investigated inertia motor

The equation of motion of the slider is thus

$$m_S \ddot{x}_S(t) = F_x(t) - F_g \sin\gamma + F_f(t). \tag{1}$$

A friction model with two discrete states of stiction and sliding is assumed in the following. During stiction, rod and slider move together, which results in

$$F_f(t) = m_S \ddot{x}_R(t) + F_g \sin\gamma - F_x(t). \tag{2}$$

Sliding begins when $F_f(t)$ exceeds the break-away force $F_{f,0}(t)$ determined by $F_c(t)$ and the coefficient of stiction μ_0:

$$|F_f(t)| > F_{f,0}(t) = \mu_0 F_c(t). \tag{3}$$

During sliding, the friction force is determined by

$$F_f(t) = \mu_d F_c \operatorname{sgn}\left(\dot{x}_R(t) - \dot{x}_S(t)\right), \tag{4}$$

where μ_d is the coefficient of sliding friction, which can be a function of the relative velocity between rod and slider. Stiction begins again when the velocities of rod and slider are equal:

$$\dot{x}_R(t) = \dot{x}_S(t). \tag{5}$$

In all following calculations and experiments, the slider is operated horizontally, i. e. with $\gamma = 0°$, with a constant contact force $F_c = F_c(t)$, and unless explicitly stated otherwise, without any external force in sliding direction, i. e. with $F_x(t) = 0$.

5 Characterization of the friction contact

When characterizing friction contacts, the measurement conditions should generally be as close as possible to the operating conditions of the investigated system [4], because friction coefficients and other parameters of one and the same friction contact can change significantly with measurement conditions [5].

In the test motor, the friction force between rod and slider could easily be measured by dragging the slider along the rod and measuring the force required to move the slider. But this setup with large movements and an approximately constant relative velocity

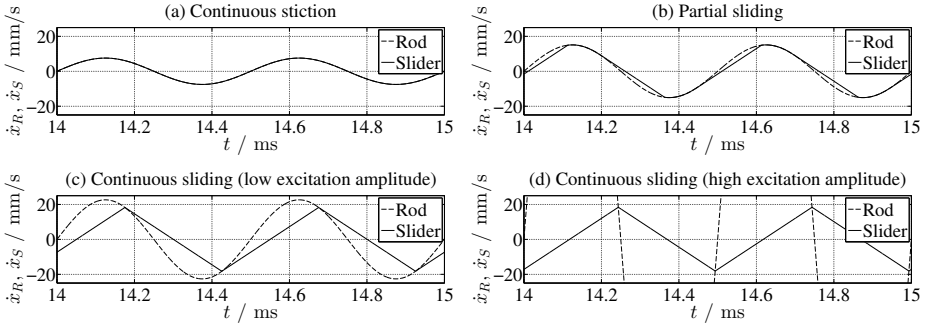

Fig. 7 Principal characteristic of the slider velocity at sinusoidal rod motion of different amplitude. Simulated for a frequency of 2000 Hz and stator amplitudes of (a) 0.6 µm, (b) 1.2 µm, (c) 1.8 µm, and (d) 18 µm.

is very different from the conditions during inertia motor operation. It is also possible to determine the friction force acting on the slider during normal motor operation from the slider acceleration, which can be derived from a laser vibrometer measurement of the slider velocity, as described in [13]. But this method is rather time-consuming and produces heavily fluctuating results.

The friction forces in the inertia motor have therefore been determined using a method based on evaluating the movement of the slider when the rod performs a sinusoidal motion: Assuming Coulomb friction, the slider velocity shows one of three characteristics depending on the excitation amplitude and frequency. Examples of these characteristics are shown in fig. 7: The slider either continuously sticks to the rod as in fig 7(a), breaks loose and slides for parts of the period as in fig. 7(b), or slides all the time as in fig. 7(c) and (d). In the first case, the slider velocity is sinusoidal. In the third case, it is triangular. This transition with increasing excitation amplitude from a sinusoidal to a triangular waveform has consequences for the mean absolute velocity and acceleration of the slider, the phase shift between the velocities of rod and slider, and the amplitudes of higher harmonics in the slider velocity. These characteristics can be evaluated in order to determine the coefficients of stiction and friction [11]. For example, the mean absolute slider acceleration $\bar{a}_{S,\mathrm{abs}}$ increases linearly with increasing excitation amplitude as long as the slider continuously sticks to the rod as in fig 7(a). If the slider is sliding all the time as in fig. 7(c) and (d), $\bar{a}_{S,\mathrm{abs}}$ equals the acceleration produced by the friction force $\mu_d F_c$, which is constant in a Coulomb friction model, cp. equation (4).

The velocities of rod and slider are measured independently. By driving the stator with a sinusoidal voltage of stepwise increasing and decreasing amplitude at a suitable fixed frequency, and evaluating each of the steps, a large number of measurement points is obtained in a short time. As an example, fig. 8 shows measured time series of the velocities of rod and slider at different excitation amplitudes. Fig. 9 shows the dynamic friction force, calculated from the mean absolute slider acceleration as

$$F_{f,d} = m_S \cdot \bar{a}_{S,\mathrm{abs}} = m_S \cdot \frac{1}{(k_2 - k_1) \cdot T} \int_{k_1 T}^{k_2 T} |\ddot{x}_S(t) - \ddot{x}_R(t)| \, \mathrm{d}t, \qquad (6)$$

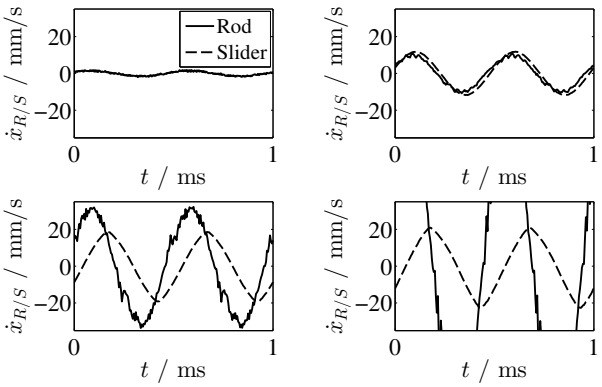

Fig. 8 Measured velocities of rod and slider. Excitation frequency 2000 Hz, excitation amplitude rising from upper left to lower right, approximately 0.1 µm, 0.8 µm, 2.5 µm, and 8.0 µm

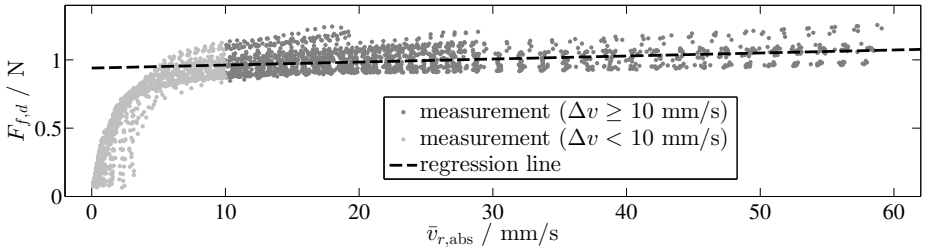

Fig. 9 Dynamic friction force $F_{f,d}$ calculated from the mean absolute slider acceleration $\bar{a}_{S,\mathrm{abs}}$ in the experiments with sinusoidal rod motion, plotted over the mean absolute relative velocity $\bar{v}_{r,\mathrm{abs}}$

for all measured cases, plotted over the individual mean absolute relative velocity

$$\bar{v}_{r,\mathrm{abs}} = \frac{1}{(k_2 - k_1) \cdot T} \int_{k_1 T}^{k_2 T} |\dot{x}_S(t) - \dot{x}_R(t)| \, \mathrm{d}t, \tag{7}$$

where T is the excitation period and k_1, k_2 are appropriately chosen whole numbers.

Other than in a Coulomb friction model, $F_{f,d}$ does not saturate with rising $\bar{v}_{r,\mathrm{abs}}$, but continuously increases. The experiments show that there is no significant phase of stiction at $\bar{v}_{r,\mathrm{abs}} \geq 10\,\mathrm{mm/s}$. In this range of $\bar{v}_{r,\mathrm{abs}}$, the friction force can thus be determined from $\bar{a}_{S,\mathrm{abs}}$ as described above. A regression line was calculated using a least squares approach. It follows the equation

$$F_{f,d}(\bar{v}_{r,\mathrm{abs}}) = 0.940\,\mathrm{N} + 2.213\,\mathrm{Ns/m} \cdot \bar{v}_{r,\mathrm{abs}}. \tag{8}$$

For a Coulomb friction model, i. e. a constant friction force, the regression yields

$$F_{f,d} = 1.01\,\mathrm{N}. \tag{9}$$

The break-away force $F_{f,0} = \mu_0 F_c$ generally has little to no influence on the characteristics of high-velocity inertia motors as these mostly use sliding friction. Several classic experiments suggest that the coefficients μ_0 and μ_d are equal in systems with

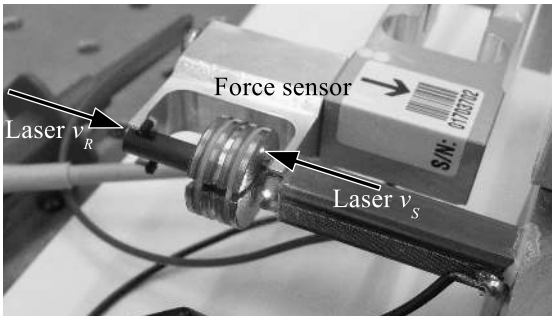

Fig. 10 Experimental setup for the determination of motor characteristics

	1st harm. ampl.	2nd harmonic ampl.	2nd harmonic phase	3rd harmonic ampl.	3rd harmonic phase	4th harmonic ampl.	4th harmonic phase
desired displacement	6.23 µm	2.43 µm	−153.7°	1.07 µm	46.9°	0.37 µm	−113.9°
voltage according to linear model	37.44 V	13.98 V	−73.1°	5.75 V	−152.1°	2.05 V	126.1°
voltage applied after iteration	36.87 V	14.09 V	−75.1°	5.76 V	−150.1°	1.97 V	140.5°

Table 1 Amplitudes and phases of the individual harmonics of one investigated signal ($f_1 = 4625\,\mathrm{Hz}$, $n = 2$, $f_n = 9250\,\mathrm{Hz}$); all phases specified relative to the 1st harmonic

large rates of change of the tangential force [25, p. 90 and references given therein]. This is the case in high-velocity inertia motors such as the investigated test motor. Because it is difficult to determine directly at conditions similar to the operation of the test motor, the break-away force is therefore assumed to equal the dynamic friction force at infinitely small relative velocity, which can be calculated as $F_{f,d}\,(\bar{v}_{r,\mathrm{abs}} = 0)$ from equation (8) or (9).

6 Experimental setup and procedure

The desired stator displacement signals can be obtained only if the electric driving signal accounts for the stator dynamics. This is achieved in two steps: First, the desired signal is passed through an inverse linear model of the stator dynamics derived from the frequency sweep shown in fig. 5, as described in [12]. The stator is then excited using the obtained electrical signal. Due to nonlinearities of the system such as hysteresis and amplitude dependence, the desired displacement profile is typically reached only roughly with this signal. Thus, in a second step, the measured rod displacement is analyzed and amplitudes and phases of the electrical signal are adjusted accordingly. Typically, one such iteration cycle is sufficient to achieve amplitude and phase errors below 1 %, respectively 1°. As an example, table 1 shows the amplitudes and phases of the individual harmonics of the desired displacement and of the excitation voltage before and after iteration for one of the investigated signals.

Fig. 10 shows the experimental setup used for the experimental determination of motor characteristics. The motor is driven so that the slider moves between the two end stops. These are connected to a force sensor which measures the reaction force $-F_x(t)$

of the end stops, cp. fig. 6. The force signal is recorded together with the velocities of rod and slider, the voltage applied to the piezoelectric actuator, and the resulting current.

All performance indicators defined in detail in the theoretical analyses in [14,15] are investigated experimentally: The steady state velocity $\bar{v}_\infty$ is determined as the mean slider velocity after the start-up phase and before the slider hits an end stop. The start-up time $t_{0.99}$, after which the motor reaches 99 % of its steady state velocity, is determined using an exponential regression function. At very low exciation frequencies, the mean motor velocity does not increase, but decrease over the first periods. In these cases, the same procedure is used to determine $t_{1.01}$, , the time after which the motor reaches 101 % of its steady state velocity. For the investigated frequencies, the steady state velocity of the motor is reached after only a few excitation periods, often even in the first period. Combined with inevitable measurement noise, this makes the start-up time the performance indicator which is most difficult to determine. Instead of the steady state smoothness indicator ς_∞ introduced in [14], its inverse, the steady state peak-to-peak ripple r_∞ of the slider velocity is investigated, because a standard definition of ripple can be used. It is determined from the measured slider velocity $\dot{x}_S(t)$ in steady state and $\bar{v}_\infty$ as

$$r_\infty = \frac{\max\left(\dot{x}_S(t)\right) - \min\left(\dot{x}_S(t)\right)}{|\bar{v}_\infty|}. \tag{10}$$

The durability indicator δ_∞ introduced in [15] describes the ratio of travelled distance and worn volume. For its calculation, the normal force F_c in the friction contact must be known. Because this force cannot be measured in the test motor, $F_c\delta_\infty$, which can be determined without knowing F_c, is calculated and compared instead. $\zeta_\infty = \bar{v}_\infty / S$ is an indicator for the energy efficiency of an inertia motor, describing the ratio of steady state velocity $\bar{v}_\infty$ and input power S. For its experimental determination, the amplitude S of the complex power is determined from the measured voltage and current of the piezoelectric actuator.

In addition to the aforementioned performance indicators, the force generation potential of the motor is investigated. The force generated by an inertia motor has been investigated by only a few researchers to date and has previously been measured by making the slider move against a spring or load cell [7,6,3,26], by driving a part directly connected to a load cell instead of a slider [29], or by lifting weights [23]. The influence of the measurement method on the results and their practical significance have not been investigated so far. A model simulation, using $F_x(t)$ as a spring force, shows that running the slider against a spring is a robust method to determine the force generation potential of an inertia motor if the spring is sufficiently soft. Fig. 11 shows the mean spring force $\bar{F}_x$ in steady state for one example setup. In this case, the critical spring stiffness is approximately 80 N/mm. At lower stiffnesses, the steady state spring force is independent of the stiffness. This method can therefore be used to determine the force generation potential of an inertia motor even if the load stiffness is not known exactly, as long as it can be assured to be below this critical value which can be identified from model simulations.

In the experiments, the motor is driven using signals containing 2, 3, or 4 harmonics with fundamental frequencies f_1 between 578 Hz and 9250 Hz. The frequency of the highest harmonic in a signal is referred to as $f_n = nf_1$. The amplitude of the excitation voltage is chosen so that the rod has a stroke of 15 µm in all of these cases.

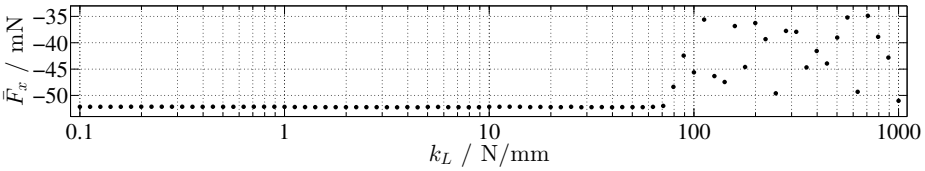

Fig. 11 Mean steady state spring force $\bar{F}_x$ calculated for different spring stiffnesses k_L

7 Results

The results of the experiments have been compared to simulations using two different fricton models derived from the characterization of the friction contact described in section 5: Model 1 uses Coulomb friction with the dynamic friction force $F_{f,d} = 1.01\,\mathrm{N}$. Model 2 uses a velocity-dependent dynamic friction force $F_{f,d}(\Delta v)$ as described by equation 8. Fig. 12 shows simulation and experimental results.

Except for the start-up time, which is difficult to determine experimentally especially at low frequencies, all experimental results are well reproducable. In almost all cases, simulation with friction model 2 produces results closer to the measurement than simulation with friction model 1. A larger relative deviation between model 2 and the measurement can only be observed in the case with the lowest fundamental frequency ($n = 4$ at $f_n = 2312\,\mathrm{Hz}$), where stiction has the largest influence on the slider motion.

8 Conclusions

The comparison of the two friction models shows that it can be important to pay attention to the dependence of the friction force on the relative velocity between the friction partners when simulating an inertia motor. Using a friction model which incorporates a velocity-dependent friction force, the simulation reproduces the measured motor characteristics well, especially at higher frequencies. Inertia motors which are constructed for high velocity usually operate at frequencies above the highest frequencies which can be investigated using the test motor. A model with a velocity-dependent friction force should thus also be appropriate for the simulation of these motors.

The experiments confirmed the theoretical findings from [14, 15], that high-velocity inertia motors should be driven with high frequencies and that two superposed sinusoidal signals are sufficient to reach high velocities. If the motor shall be able to generate larger forces, signals with more harmonics should be used. The driving frequency has little influence on the generated force above a relatively low threshold.

References

1. Anders, M., Thaer, M., Heiden, C.: Simple micropositioning devices for STM. Surf. Sci. **181**(1–2), 176–182 (1987)
2. Bansevicius, R., Blechertas, V.: Multi-degree-of-freedom ultrasonic motors for mass-consumer devices. J. Electroceram. **20**(3), 221–224 (2008)
3. Belly, C., Porchez, T., Bagot, M., Claeyssen, F.: Improvement of linear and rotative stepping piezo actuators using design and control. In: ACTUATOR 12 Conf. Proc., pp. 246–249. Wirtschaftsförderung Bremen, Bremen (2012)

4. Bergander, A., Breguet, J.M.: A testing mechanism and testing procedure for materials in inertial drives. In: 2002 Int. Symp. Micromechatronics and Human Science, Nagoya, Japan, pp. 213–218. IEEE (2002)
5. Blau, P.J.: Scale effects in sliding friction: An experimental study. In: I.L. Singer, H.M. Pollock (eds.) Fundamentals of Friction: Macroscopic and Microscopic Processes, pp. 523–534. Kluwer, Dordrecht (1992)
6. Cheng, C., Hung, S.: The design and characteristic research of a dual-mode inertia motor. In: 2011 IEEE/ASME Int. Conf. Advanced Intelligent Mechatronics, Budapest, pp. 605–610 (2011)
7. Edeler, C., Fatikow, S.: Open loop force control of piezo-actuated stick-slip drives. Int. J. Intelligent Mechatronics and Robotics **1**, 1–19 (2011)
8. Hamming, R.W.: Numerical Methods for Scientists and Engineers, republ. 2nd edn. Dover, New York (1986)
9. Henderson, D.A.: Linear drive systems and methods thereof (patent application US 8059346 A1) (2011)
10. Higuchi, T., Hojjat, Y., Wanatabe, M.: Micro actuators using recoil of an ejected mass. In: Micro Robots and Teleoperators Workshop, Hyannis, Massachusetts. IEEE (1987)
11. Hunstig, M.: Konzeption, Ansteuerung und Eigenschaften schneller piezoelektrischer Trägheitsmotoren. No. 2 in Schriften des Lehrstuhl für Mechatronik und Dynamik. Shaker, Aachen (2014)
12. Hunstig, M., Hemsel, T., Sextro, W.: Improving the performance of piezoelectric inertia motors. In: ACTUATOR 10 Conf. Proc., pp. 657–661. Wirtschaftsförderung Bremen, Bremen (2010)
13. Hunstig, M., Hemsel, T., Sextro, W.: Modelling the friction contact in an inertia motor. J. Intel. Mat. Syst. Str. **24**(11), 1380–1391 (2013)
14. Hunstig, M., Hemsel, T., Sextro, W.: Stick-slip and slip-slip operation of piezoelectric inertia drives. Part I: Ideal excitation. Sens. Actuators, A **200**, 90–100 (2013)
15. Hunstig, M., Hemsel, T., Sextro, W.: Stick-slip and slip-slip operation of piezoelectric inertia drives—Part II: Frequency-limited excitation. Sens. Actuators, A **200**, 79–89 (2013)
16. Lee, J., Kwon, W.S., Kim, K.S., Kim, S.: A novel smooth impact drive mechanism actuation method with dual-slider for a compact zoom lens system. Rev. Sci. Instrum. **82**, 085,105 (2011)
17. Matsusaka, K., Ozawa, S., Yoshida, R., Yuasa, T., Souma, Y.: Ultracompact optical zoom lens for mobile phone. In: Proc. SPIE, vol. 6502, p. 650203 (2007)
18. Morita, T., Murakami, H., Yokose, T., Hosaka, H.: A miniaturized resonant-type smooth impact drive mechanism actuator. Sens. Actuators, A **178**, 188–192 (2012)
19. Morita, T., Nishimura, T., Yoshida, R., Hosaka, H.: Resonant-type SIDM actuator operating at lower input voltages. Jpn. J. Appl. Phys. (52), 07HE05 (2013)
20. Nishimura, T., Hosaka, H., Morita, T.: Resonant-type smooth impact drive mechanism (SIDM) actuator using a bolt-clamped langevin transducer. Ultrasonics **52**(1), 75–80 (2012)
21. Okamoto, Y., Yoshida, R.: Development of linear actuators using piezoelectric elements. Electronics and Communications in Japan, Part 3 **81**(11), 11–17 (1998)
22. Paik, D.S., Yoo, K.H., Kang, C.Y., Cho, B.H., Nam, S., Yoon, S.J.: Multilayer piezoelectric linear ultrasonic motor for camera module. J. Electroceram. **22**(1), 346–351 (2009)
23. Pak, M., Nasseri, A.: Load-velocity characteristics of a stick-slip piezo actuator. In: ACTUATOR 12 Conf. Proc., pp. 755–756. Wirtschaftsförderung Bremen, Bremen (2012)
24. Pohl, D.W.: Dynamic piezoelectric translation devices. Rev. Sci. Instrum. **58**(1), 54–57 (1987)
25. Richardson, R., Nolle, H.: Surface friction under time-dependent loads. Wear **37**(1), 87–101 (1976)
26. Suzuki, M., Hosaka, H., Morita, T.: Resonant-type smooth impact drive mechanism actuator with two langevin transducers. Adv. Robotics **26**(3–4), 277–290 (2012)
27. Tuncdemir, S., Ural, S.O., Koc, B., Uchino, K.: Design of translation rotary ultrasonic motor with slanted piezoelectric ceramics. Jpn. J. Appl. Phys. **50**(2), 027,301 (2011)
28. Uchino, K.: Piezoelectric motors for camera modules. In: ACTUATOR 08 Conf. Proc., pp. 157–160. Hanseatische Veranstaltungs-GmbH, Bremen (2008)
29. Yokose, T., Hosaka, H., Morita, T.: Improvement of miniaturized resonant type SIDM actuator. In: 2012 IEEE Int. Ultrasonics Symp., pp. 1810–1813. IEEE (2012)

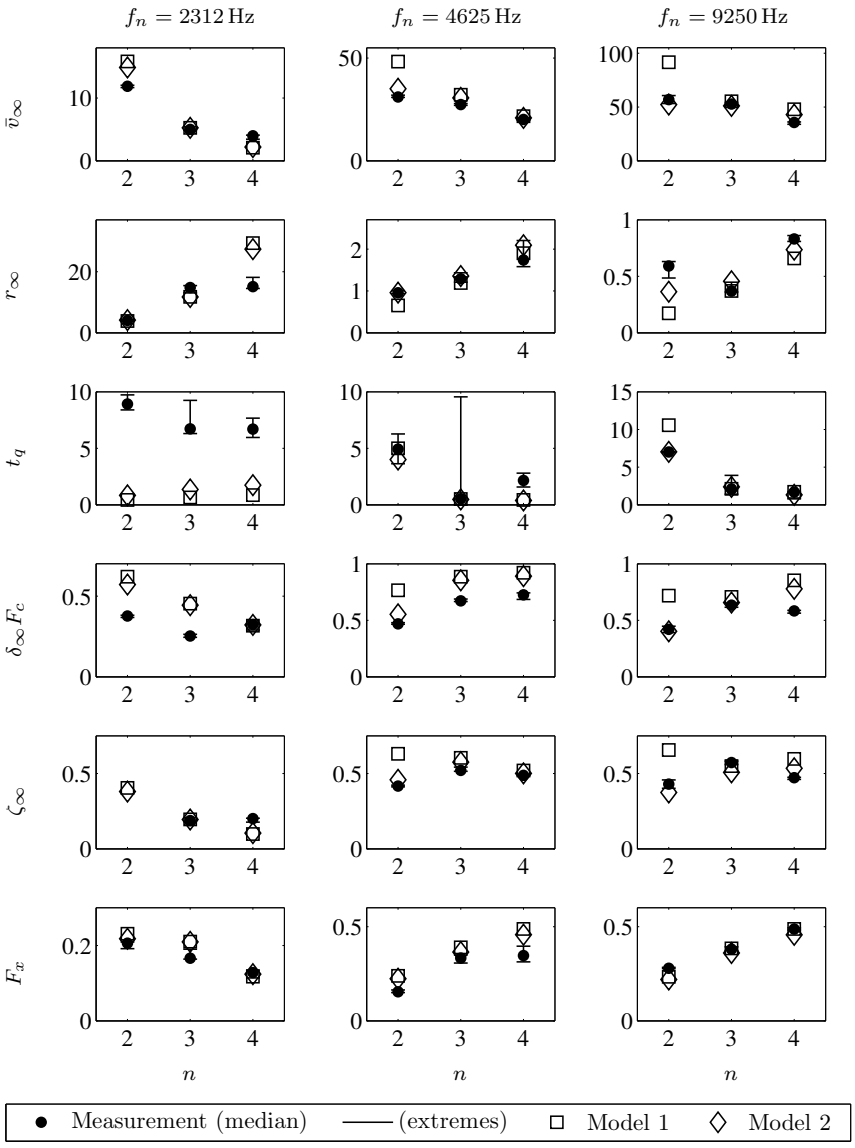

Fig. 12 Steady state velocity $\bar{v}_\infty$, velocity ripple r_∞, start-up time t_q (with $q = 0.99$ or 1.01), durability indicator $\delta_\infty F_c$, velocity to input power ratio ζ_∞, and maximum load force F_x of the test motor, determined experimentally and in simulations with different numbers of harmonics n and different maximum frequencies f_n